

Interacting topological phases in thin films of topological mirror Kondo insulators

Rui-Xing Zhang,¹ Cenke Xu,² and Chao-Xing Liu¹

¹*Department of Physics, The Pennsylvania State University, University Park, Pennsylvania 16802*

²*Department of Physics, University of California, Santa Barbara, CA 93106*

(Dated: March 2, 2022)

We study the interaction effects on thin films of topological mirror Kondo insulators (TMKI), where the strong interaction is expected to play an important role. Our study has led to the following results: (1) We identify a rich phase diagram of non-interacting TMKI with different mirror Chern numbers in the monolayer and bilayer thin films; (2) We obtain the phase diagram with interaction and identify the regimes of interaction parameters to mimic bosonic symmetry protected topological phases with either gapless bosonic modes or spontaneous mirror symmetry breaking at the boundary; (3) For the spontaneous mirror symmetry breaking boundary, we also study various domain-wall defects between different mirror symmetry breaking order parameters at the boundary. Our results reveal that the thin film TMKI serves as an intriguing platform for the experimental studies of interacting topological phases.

PACS numbers:

I. INTRODUCTION

A topological state is usually characterized by certain type of topological invariant. As a consequence of their “nontrivial topology”, topological states possess gapless modes at the boundary of the sample¹. Recently, intense research interests have been focused on the role of symmetry in the classification of topological states and it was shown that symmetries substantially enrich the family of topological states. These new topological states, known as symmetry protected topological (SPT) states^{2,3}, have been proposed for different types of symmetries in electronic systems, including time-reversal invariant topological insulators (TIs)⁴⁻⁷, topological superconductors⁷, topological crystalline insulators^{8,9} and superconductors¹⁰. With the help of the state-of-the-art first principles calculations, these theoretical predictions have successfully led to the experimental discovery of different types of SPT phases in electronic systems. Examples include two dimensional (2D) TIs in HgTe/CdTe quantum wells^{11,12}, InAs/GaSb quantum wells^{13,14}, *et al*, three dimensional (3D) TIs in Sb/Bi alloy, Bi or Sb-based chalcogenides^{5,15-17}, *et al*. More recently, it has been proposed that SPT phases can also be realized in photonic systems^{18,19}.

Theoretically, it has been shown that strong interaction can significantly change the classification of topological insulators/superconductors. The first example is the one dimensional (1D) interacting topological superconductor. For free fermions, 1D topological superconductors with time-reversal symmetry \mathcal{T} and $\mathcal{T}^2 = +1$ (BDI class)²⁰ has a \mathbb{Z} classification (which is characterized by an arbitrary integer number of Majorana fermion zero modes at its boundary), but Fidkowski and Kitaev^{21,22} pointed out that appropriate \mathcal{T} -invariant interactions can render the ground state of eight Majorana fermion zero modes gapped and nondegenerate, which implies that the classification of these TSCs is reduced from \mathbb{Z} to \mathbb{Z}_8 under interaction. Examples for such “inter-

action reduced classification” in higher dimensions were also found²³⁻³⁰.

Unlike their fermionic analogues, strong interaction is demanded to realize bosonic SPT (BSPT) states. However, so far theoretical studies for BSPT states have been focused on theoretical classification and field theory descriptions^{2,3,31-34}, but most of the lattice models proposed for BSPT states in two and three dimensions are usually complex and unrealistic. Very recently, it was proposed that interacting BSPT phases can be realized by introducing interactions to a 2D quantum spin Hall system with two channels of helical edge states³⁵ and total spin S^z conservation. These BSPT states which originate from fermionic systems not only have gapless bosonic edge modes, but also are separated from the trivial state with a purely “bosonic quantum phase transition”, which has been observed numerically^{36,37}. It was also shown theoretically that the bilayer graphene under both a strong out-of-plane magnetic field and Coulomb interaction mimics much of the physics of a BSPT state³⁵. A natural question is whether similar physics can exist in other condensed matter systems.

In this work, we explore interacting topological phases, in particular the possibility of BSPT state, in topological Kondo insulators³⁸, which is a class of topological insulator materials with strong interactions. In Kondo insulators, a small band gap opens up due to the hybridization between localized f-electrons and conducting d-electrons. It turns out that this hybridization gap is topologically non-trivial, making this class of materials also time-reversal invariant TIs. Topological nature of this class of materials, including SmB_6 and YbB_6 , has recently been experimentally confirmed by Ref. [39–44]. More recent studies reveal that mirror symmetry also plays a role in some Kondo insulators, thus we will refer to these systems as topological mirror Kondo insulators (TMKI). For example, it is found that the topological nature of SmB_6 can either be protected by time-reversal symmetry (\mathbb{Z}_2 class)⁴⁵ or by mirror symmetry

(\mathbb{Z} class without interaction)⁹. Due to the existence of f-electrons near the Fermi energy, interaction is quite strong in Kondo insulators. However, so far the studies on topological phases in TMKIs have essentially followed the paradigm of free electron TIs. Therefore, it is natural to ask if interacting SPT phases, especially BSPT states that are qualitatively beyond the free fermion limit, can be realized in TMKIs.

To address this question, we consider thin films of TMKIs, such as SmB_6 , and study topological phases of this 2D system. We assume that the thin film is grown along the direction with mirror symmetry, in which mirror Chern number⁹, an integer topological invariant defined based on mirror symmetry, can be utilized to characterize the topological nature of this system. By tuning the thickness and hybridization parameters between different orbitals of the thin films, we find a rich phase diagram, which stems from the competition between strong hybridization effect and quantum confinement effect (QCE). Topological phases with different mirror Chern numbers (as large as 6) can be realized in the phase diagram. Furthermore, we show that in addition to the charge $U(1)$ symmetry and mirror symmetry, another effective $U(1)$ symmetry can be defined, which operates oppositely in two mirror parity subspaces and is dubbed the “pseudo-spin” $U(1)_m$ symmetry in this paper, at the single particle level. Based on the 2D model, we further study the interaction effect on the topological mirror insulator phase with two copies of helical edge states (mirror Chern number being 2) based on the Abelian bosonization formalism. We notice that the “pseudo-spin” $U(1)_m$ symmetry and mirror symmetry are playing different roles in the interacting system. If interaction preserves the “pseudo-spin” $U(1)_m$ symmetry, the system can be driven into the BSPT phase with only one gapless bosonic edge mode and hence central charge $c = 1$; if interaction breaks the “pseudo-spin” $U(1)_m$ symmetry while preserving the mirror symmetry, the edge states will be gapped out due to spontaneous breaking of the mirror symmetry when the interaction is relevant. Depending on the form of interaction, different types of interacting phases are discussed and the conditions for the interacting BSPT phase are identified.

II. TWO DIMENSIONAL TCI PHASES IN TMKI THIN FILMS

A. Model of TMKI thin films

We start from a description of the 2D model for the TMKI thin films. Following Ref. [46,47] where various tight-binding models of SmB_6 have been summarized and discussed, we consider a four band model described in Ref. [46,48] due to its simplicity. This model has been shown to reproduce energy dispersion from more complicated multi-band models, as well as the first principles calculations⁴⁶. We notice that the obtained spin

texture from this model is not exactly the same as that from more sophisticated models⁴⁶, but this difference is not essential for the physical mechanism discussed below. This model describes a cubic Kondo lattice with spinful d-orbital and f-orbital electrons that are hybridized by inter-orbital coupling. The basis function for this four band model is: $|\Psi\rangle = (d_\uparrow, d_\downarrow, f_\uparrow, f_\downarrow)^T$ ⁴⁸. The bulk model shows 3D topological crystalline insulating phases with a non-trivial mirror Chern number at certain mirror invariant planes^{46,48}. Here we consider the thin film configuration stacking along the direction perpendicular to the mirror invariant plane. The intralayer part of Hamiltonian (H_{00}) and interlayer part of Hamiltonian (H_{01}) are given by

$$H_{00} = \begin{pmatrix} h_{00}^d & \Phi_{00} \\ \Phi_{00}^\dagger & h_{00}^f \end{pmatrix}, \quad H_{01} = \begin{pmatrix} h_{01}^d & \Phi_{01} \\ \Phi_{10}^\dagger & h_{01}^f \end{pmatrix} \quad (1)$$

where

$$\begin{aligned} h_{00}^d &= (-2t_d(c_1 + c_2) - 4t'_d c_1 c_2) \sigma_0 \\ h_{00}^f &= (e_f - 2t_f(c_1 + c_2) - 4t'_f c_1 c_2) \sigma_0 \\ h_{01}^{d(f)} &= (-t_{d(f)} - 2t'_{d(f)}(c_1 + c_2) - 4t''_{d(f)} c_1 c_2) \sigma_0 \\ \Phi_{00} &= -2[s_1 \sigma_x (V_1 + V_2 c_2) + s_2 \sigma_y (V_1 + V_2 c_1)] \\ \Phi_{01} &= -[s_1 V_2 \sigma_x + s_2 V_2 \sigma_y + \frac{1}{i} \sigma_z (V_1 + V_2 (c_1 + c_2))]. \end{aligned} \quad (2)$$

We label $c_i = \cos k_i$ and $s_i = \sin k_i$ with $i = 1, 2, 3$ for short. We only focus on the monolayer case (described by H_m) and the bilayer case (described by H_b) with the corresponding Hamiltonians given by

$$H_m = H_{00}, \quad (3)$$

$$H_b = \begin{pmatrix} H_{00} & H_{01} \\ H_{01}^\dagger & H_{00} \end{pmatrix}, \quad (4)$$

respectively. In general, an n -layer ($n = 1, 2, 3, \dots$) thin film model can be constructed in a similar way.

Before we study the details of topological phase transition in monolayer and bilayer films of TMKI, we first discuss symmetry properties for our system. For a 2D thin film, out-of-plane mirror symmetry m_z plays a central role in protecting topological crystalline phases. Under the basis $|\Psi\rangle$, the bulk mirror operation is $m_z = i\tau_z \otimes \sigma_z$ with τ and σ for the orbital and spin degree of freedom. Starting from the bulk mirror operation m_z , it is straightforward to write down the mirror operations for monolayer model (M_z^m) and bilayer model (M_z^b) as

$$\begin{aligned} M_z^m &= m_z = i\tau_z \otimes \sigma_z \\ M_z^b &= \alpha_x \otimes m_z = i\alpha_x \otimes \tau_z \otimes \sigma_z, \end{aligned} \quad (5)$$

where α_i denotes the Pauli matrix of layer degree of freedom in the bilayer case. In a mirror symmetric system, all the eigen-states can be characterized by their mirror parities (the eigen-values of mirror operators) and two

subspaces characterized by opposite mirror parities are decoupled. When time-reversal symmetry is present, a non-zero net Chern number C is forbidden, while mirror symmetry allows a possible non-vanishing Chern number $C_{\pm i}$ in each mirror subspace (with mirror eigenvalue being either $+i$ or $-i$), leading to the topological mirror insulator phase. In general, we have

$$\begin{aligned} C &= C_{+i} + C_{-i} = 0 \\ C_m &= (C_{+i} - C_{-i})/2 = C_{+i}. \end{aligned} \quad (6)$$

Therefore, to understand the topology of the whole system (with time-reversal symmetry), it is sufficient for us to check only the Chern number in one mirror subspace (for example, C_{+i} for the $+i$ mirror subspace).

Here we would like to point out an interesting emergent symmetry that is usually ignored in previous discussions of topological mirror insulators. With mirror symmetry, since two mirror subspaces are decoupled, the full Hamiltonian is block diagonal under the basis with definite mirror parities. As a result, we can perform different $U(1)$ phase transformations on each mirror subspace, while leaving the Hamiltonian invariant under such operation. In analogy to spin $U(1)$ symmetry, we call this emergent $U(1)_m$ symmetry as a ‘‘pseudo-spin’’ symmetry. The mirror symmetry and pseudo-spin symmetry $U(1)_m$ are essentially different, but they cannot be distinguished in the non-interacting limit. Their difference will be clarified when we consider interaction effects in a later section.

B. Phase diagram of a monolayer system

In this section we discuss possible topological phase transitions (TPTs), as well as the phase diagram, as a function of the off-block-diagonal coefficients V_1 and V_2 in Eq. (1), which control the hybridization gap between d-electrons and f-electrons, in a monolayer TMKI thin film. We find that TPTs are determined by two conditions

$$\begin{aligned} h_{00}^d &= h_{00}^f & (7) \\ \Phi_{00}(k_x, k_y) &= 0 & (8) \end{aligned}$$

in H_{00} (Eq. (3)). We generally search for solutions for the above two equations at high symmetry lines in the Brillouin zone (BZ). The explicit expression for Eq. (7) is written as

$$2(t_d - t_f)(c_1 + c_2) + 4(t'_d - t'_f)c_1c_2 + e_f = 0, \quad (9)$$

which is simplified to

$$6(c_1 + c_2) - 6c_1c_2 - 5 = 0, \quad (10)$$

with the parameters $t_d = 1, t'_d = -0.5, e_f = -2, t_f = -\frac{1}{5}t_d, t'_f = -\frac{1}{5}t'_d$ according to Ref. [46]. Eq. (10) can be solved and we find the following solutions: (1) $(k_x, k_y) = (\pi, \cos^{-1} \frac{11}{12})$ along the X - M line ($k_x = \pi, k_y = k$); (2)

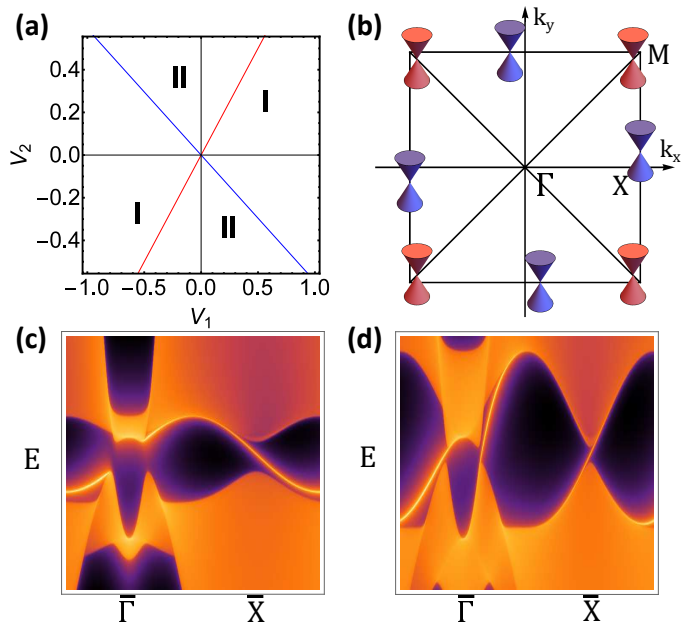


FIG. 1: Topological phase diagram in the monolayer system. Red (blue) line represents TPT happening at X - M (Γ - M) line. In Fig. (b), the blue (red) Dirac cone represents the position of a TPT characterized by the blue (red) critical line in (a). Region I is a TCI phase with mirror Chern number -1 , while region II is a TCI phase with mirror Chern number $+3$. Edge dispersions are calculated using iterative Green function method for a semi-infinite configuration: (c) Region I with $C_m = -1$, (d) Region II with $C_m = +3$.

$(k_x, k_y) = (\cos^{-1}(1 - \frac{\sqrt{6}}{6}), \cos^{-1}(1 - \frac{\sqrt{6}}{6}))$ along the M - Γ line ($k_x = k_y = k$); (3) $(k_x, k_y) = (\cos^{-1} \sqrt{\frac{5}{6}}, \pi - \cos^{-1} \sqrt{\frac{5}{6}})$ along the Y - X line ($k, \pi - k$). Here we only list the solutions in the first quarter of the BZ and the solutions in other parts of the BZ can be obtained by performing four-rotation rotation. On the other hand, Eq. (8) can be simplified as

$$\begin{aligned} \sin k_x (V_1 + V_2 \cos k_y) &= 0 \\ \sin k_y (V_1 + V_2 \cos k_x) &= 0, \end{aligned} \quad (11)$$

which can be satisfied by $V_1 = V_2$ for the X - M line and $V_1 = -(1 - \frac{\sqrt{6}}{6})V_2$ at $(k_x, k_y) = (\cos^{-1}(1 - \frac{\sqrt{6}}{6}), \cos^{-1}(1 - \frac{\sqrt{6}}{6}))$ along the M - Γ line. Combining the solutions from the Eq. (7) and (8) leads to two types of TPTs: (1) When $V_1 = V_2$, TPT happens at $(k_x, k_y) = (\pi, \cos^{-1} \frac{11}{12})$ along the X - M line; (2) When $V_1 = -(1 - \frac{\sqrt{6}}{6})V_2$, TPT happens at $(k_x, k_y) = (\cos^{-1}(1 - \frac{\sqrt{6}}{6}), \cos^{-1}(1 - \frac{\sqrt{6}}{6}))$ along the Γ - M line. Because of the four-fold rotation symmetry, each of the TPTs will occur at four different momenta simultaneously.

The phase diagram is summarized in Fig. 1 (a), where the red line shows the TPTs at the X - M line while the blue line is for the TPTs at the Γ - M line. The blue (red) Dirac cones in Fig. 1 (b) depict the exact positions of the

TPTs represented by the blue (red) line in Fig. 1 (a). To identify the mirror Chern number in the region I and II, we calculate the edge state dispersion in a ribbon configuration along the y direction for the mirror subspace with the mirror parity $+i$ in Fig. 1 (c) and (d). The number and chirality of chiral edge states correspond to both the absolute value and the sign of bulk mirror Chern number according to the bulk-boundary correspondence. The phase in the region I (Fig. 1 (c)) possesses mirror Chern number $C_m = C_{+i} = -1$, while that in the region II (Fig. 1 (d)) carries $C_m = C_{+i} = 3$. The change of the Chern number $|\Delta C_m| = 4$ across the TPTs is due to the four-fold rotation symmetry of the system.

C. Phase diagram of a bilayer system

In the monolayer system, TPTs are controlled by hybridization effects. In contrast, an additional ingredient, the QCE, also plays a role in the TPT of a bilayer system. QCE is determined by the inter-layer hopping (the off-block-diagonal term) of the Hamiltonian. To make connection between monolayer and bilayer films, we introduce an inter-layer coupling parameter $\lambda \in [0, 1]$ between two layers and re-write the Hamiltonian as

$$H_b(\lambda) = \begin{pmatrix} H_{00} & \lambda H_{01} \\ \lambda H_{01}^\dagger & H_{00} \end{pmatrix}. \quad (12)$$

When $\lambda = 0$, two layers are completely decoupled, and $H_b(0)$ describes the monolayer system with the phase diagram shown in Fig. 1 (a). When $\lambda = 1$, two layers are strongly coupled, and $H_b(1)$ reproduces the bilayer system H_b in Eq. (4). Therefore, by tuning λ continuously, we can understand the evolution of the energy spectrum from the monolayer system to the bilayer system.

We emphasize that the M_z^b mirror parity of an eigenstate in the bilayer film is not directly related to the M_z^m mirror parity for an eigenstate in each monolayer. A nonzero λ introduces interlayer coupling, resulting in the formation of bonding and anti-bonding states. Let us denote $|+i(-i), n\rangle$ as the mirror even (odd) state of the monolayer mirror operation M_z^m for the n th layer ($n = 1, 2$). For the bilayer system, the even and odd states under M_z^b are the linear combinations of $|\pm i, n\rangle$:

$$\begin{aligned} \langle M_z^b \rangle = +i & : \frac{1}{\sqrt{2}}(|+i, 1\rangle + |+i, 2\rangle) \\ & \frac{1}{\sqrt{2}}(|-i, 1\rangle - |-i, 2\rangle) \\ \langle M_z^b \rangle = -i & : \frac{1}{\sqrt{2}}(|-i, 1\rangle + |-i, 2\rangle) \\ & \frac{1}{\sqrt{2}}(|+i, 1\rangle - |+i, 2\rangle). \end{aligned} \quad (13)$$

Therefore, starting from any M_z^m mirror eigen-state, one can obtain both even and odd M_z^b mirror eigen state of the bilayer system by making linear combination of the states in two layers.

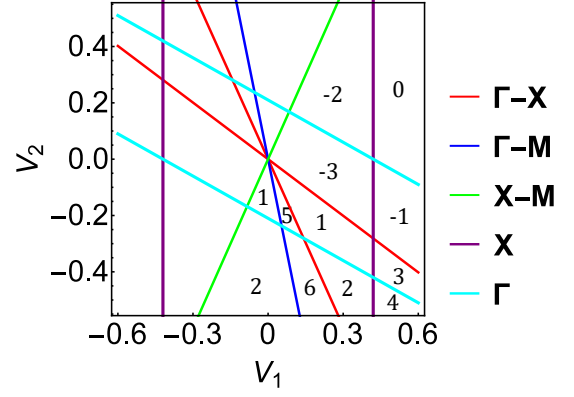


FIG. 2: Topological phase diagram for the bilayer system. TPT critical lines are plotted using different color, as shown in the legend. The numbers shown in the figure are the corresponding mirror Chern numbers.

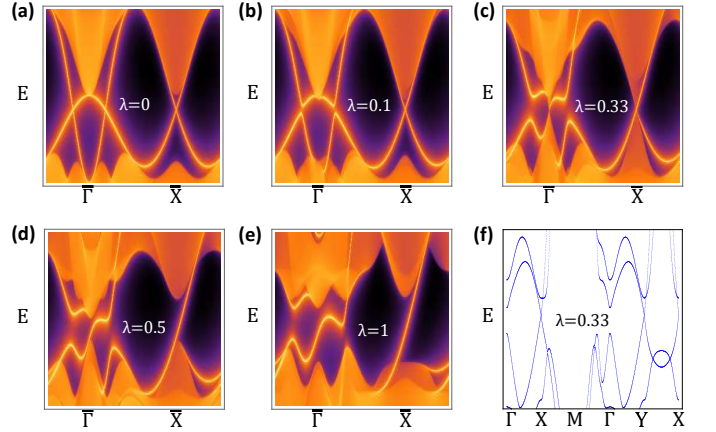


FIG. 3: Edge dispersion plots of the bilayer system with a different layer coupling λ are plotted in (a) to (e). In (f), we plot the bulk dispersion exactly at the topological phase transition.

We now map out the phase diagram of the bilayer system numerically and mirror Chern numbers are marked for different phases in Fig. 2. As a result of the combination of QCE and hybridization effect, TPTs can occur either along some high symmetry lines (e.g. Γ - X , Γ - M and X - M lines) or at some high symmetry points (e.g. X and Γ), as shown by lines with different colors in Fig. 2. Thanks to the four-fold rotation symmetry of the cubic lattice, TPTs along the lines Γ - X , Γ - M and X - M , labeled by red, blue and green lines in Fig. 2, will change the mirror Chern number by ± 4 . In contrast, TPTs at the high symmetry points Γ (X) will change the mirror Chern number by ± 1 (± 2), which are labeled by the cyan (purple) lines in Fig. 2. Due to the multiple TPTs in the bilayer system, we find that the mirror Chern number can be as large as $C_m = 6$ in the phase diagram that has been mapped out.

As an example, we track the formation of a $C_m = 2$ TCI phase (e.g. $V_1 = 0, V_2 = -0.3$) based on our

layer construction scheme by varying λ from 0 to 1 in Eq. (12). Here we choose the same set of parameters for each monolayer that belongs to the region II in Fig. 1 with a mirror Chern number $C_m = +3$. As discussed above, the eigen state with a definite mirror parity in the bilayer system is a linear combination of the eigen-states with both even and odd mirror parities in the monolayer systems. As a result, for a small λ ($\lambda = 0.1$), we find a trivial phase ($C_m = 0$) in the new $+i$ mirror subspace as shown in Fig. 3 l(b) (The gapless edge modes in Fig. 3 (a) are because two layers are decoupled for $\lambda = 0$ in the bilayer system). By tuning λ , the system undergoes a TPT at $\lambda = 0.33$, where the bulk band gap closes at both X and Y in the BZ, as shown in Fig. 3 (f). As a consequence, the mirror Chern number C_m is changed by 2, giving rise to the topological mirror insulator phase with $C_m = 2$ for $\lambda > 0.33$. As shown in Fig. 3 (d) and (e) for $\lambda = 0.5$ and $\lambda = 1$, two chiral gapless edge modes exist in the mirror parity subspace $+i$ with one of them around $\bar{\Gamma}$ (projected from Y in the bulk BZ), while the other around \bar{X} in the edge BZ. Taking into account the other mirror parity subspace ($-i$), two copies of helical edge modes exist in this bilayer system for $\lambda = 1$.

To conclude, we have demonstrated the bilayer model of a TMKI as a playground for 2D topological mirror insulator phases with various mirror Chern numbers. Different from either monolayer model or bulk model, the richness of topological mirror insulator phases in bilayer TMKI originates from the interplay between hybridization effect and QCE. Our layer construction scheme can be generalized to multiple-layer systems and thus, topological phases with higher mirror Chern numbers are expected to exist and can be tuned by the thickness of thin films. Next we will study the interaction effect in the bilayer system with the mirror Chern number $C_m = 2$ (two copies of helical edge modes).

III. INTERACTING EDGE STATES OF 2D TMKIS

In this section, we will discuss interacting physics at the 1D edge of 2D TMKIs. With the presence of interactions, previous studies have shown that the topological classification of 2D TMKI will be reduced from \mathbb{Z} to \mathbb{Z}_4 ^{49,50} in the case that the pseudo-spin symmetry $U(1)_m$ is broken while the mirror symmetry is preserved by the interaction. Similar change of topological classification should occur in our phase diagram (Fig. (2)). Our proposed TMKI thin film system with high mirror Chern numbers provides us an ideal platform to test the reduction of topological classification both theoretically and experimentally.

In this section, our main interest focuses on another intriguing aspect of interacting topological phases. In a recent paper³⁵, it was proposed that a BSPT phase protected by $U(1)_c \times U(1)_s$ symmetry can be realized in a bilayer graphene system under Coulomb interaction and

a strong magnetic field. Here $U(1)_c$ and $U(1)_s$ denote $U(1)$ symmetries corresponding to charge conservation and spin conservation, respectively. Graphene under a strong magnetic field becomes a quantum spin Hall insulator⁵¹, which was recently demonstrated experimentally⁵². Due to the similarities between a quantum spin Hall insulator and a 2D topological mirror insulator, it is natural to ask whether BSPT states could occur in our systems. With Abelian bosonization, we will discuss possible realization of BSPT states, as well as other related interacting phases. For this purpose, we will focus on a 2D TMKI phase with the mirror Chern number $C_m = 2$ in the rest of our discussions.

A. Abelian bosonization of interacting edge states of 2D TMKIs

The low energy physics at the edge of a $C_m = 2$ TMKI is well captured by the following non-interacting two-channel helical Luttinger liquid model

$$H_0 = \frac{v_f}{2} \sum_{l=1,2} [\psi_{l,L}^\dagger i\partial_x \psi_{l,L} - \psi_{l,R}^\dagger i\partial_x \psi_{l,R}], \quad (14)$$

with the channel index $l = 1, 2$. As shown in Fig. 3 (e), we can define l as the valley index and label the helical edge modes at $\bar{\Gamma}$ (\bar{X}) with $l = 1$ ($l = 2$). L (R) denotes the left mover (right mover) of chiral fermions in the even (odd) mirror subspace since mirror parity is locked to the direction of velocity of the edge states. The Abelian bosonization of the Hamiltonian (Eq. (14)) has been discussed in Ref. [35]. To keep the current paper self-contained, we briefly review the bosonization scheme as follows:

$$\begin{aligned} \psi_{l,R} &\sim e^{i2\sqrt{\pi}\chi_{l,R}} \\ \psi_{l,L} &\sim e^{-i2\sqrt{\pi}\chi_{l,L}}, \end{aligned} \quad (15)$$

where χ are chiral bosonic fields. We introduce bosonic dual variables θ_l and ϕ_l as

$$\begin{aligned} \phi_l &= \chi_{l,R} + \chi_{l,L} \\ \theta_l &= -\chi_{l,R} + \chi_{l,L}, \end{aligned} \quad (16)$$

and write the fermionic density operators in terms of dual variables as

$$\begin{aligned} \rho_{R,l} &= \frac{1}{2\sqrt{\pi}} \partial_x (\phi_l - \theta_l) \\ \rho_{L,l} &= \frac{1}{2\sqrt{\pi}} \partial_x (\phi_l + \theta_l). \end{aligned} \quad (17)$$

Finally, we define the bonding and anti-bonding states between different channels as

$$\begin{aligned} \phi_+ &= \frac{1}{\sqrt{2}}(\phi_1 + \phi_2), \quad \phi_- = \frac{1}{\sqrt{2}}(\phi_1 - \phi_2) \\ \theta_+ &= \frac{1}{\sqrt{2}}(\theta_1 + \theta_2), \quad \theta_- = \frac{1}{\sqrt{2}}(\theta_1 - \theta_2). \end{aligned} \quad (18)$$

The free fermion Hamiltonian (Eq. (14)) can be transformed into a free boson Hamiltonian in terms of bosonic variables ϕ_{\pm} and θ_{\pm} . In the bosonic Hamiltonian, two-body interaction terms, which can be explicitly written in terms of density operators, can renormalize Fermi velocities and Luttinger parameters. These interaction terms include

$$\begin{aligned} H_1 &= \sum_{l=1,2} g_1 \rho_{l,L} \rho_{l,R} \\ &= \frac{g_1}{4\pi} [(\partial_x \phi_-)^2 + (\partial_x \phi_+)^2 - (\partial_x \theta_-)^2 - (\partial_x \theta_+)^2] \\ H_2 &= \sum_{i \neq j} g_2 (\rho_{i,R} \rho_{j,L} + \rho_{i,L} \rho_{j,R}) \\ &= \frac{g_2}{4\pi} [(\partial_x \phi_+)^2 - (\partial_x \phi_-)^2 + (\partial_x \theta_-)^2 - (\partial_x \theta_+)^2]. \end{aligned} \quad (19)$$

Together with Eq. (14), the full harmonic Hamiltonian of bosons is given by

$$H_{\pm} = \frac{v_{\pm}}{2} [K_{\pm} (\partial_x \phi_{\pm})^2 + \frac{1}{K_{\pm}} (\partial_x \theta_{\pm})^2] \quad (20)$$

with the corresponding Luttinger parameters

$$\begin{aligned} K_- &= \sqrt{\frac{v_f + \frac{g_1}{2\pi} - \frac{g_2}{2\pi}}{v_f - \frac{g_1}{2\pi} + \frac{g_2}{2\pi}}} \\ K_+ &= \sqrt{\frac{v_f + \frac{g_1}{2\pi} + \frac{g_2}{2\pi}}{v_f - \frac{g_1}{2\pi} - \frac{g_2}{2\pi}}}. \end{aligned} \quad (21)$$

Now let us consider scattering that corresponds to anharmonic terms in the Hamiltonian. These terms include

$$\begin{aligned} H_{\alpha_1} &= \alpha_1 \psi_{1,L}^{\dagger} \psi_{1,R} \psi_{2,R}^{\dagger} \psi_{2,L} + h.c. \\ &\sim \alpha_1 \cos 2\sqrt{2\pi} \phi_- \\ H_{\alpha_2} &= \alpha_2 \psi_{1,L}^{\dagger} \psi_{2,R} \psi_{1,R}^{\dagger} \psi_{2,L} + h.c. \\ &\sim \alpha_2 \cos 2\sqrt{2\pi} \theta_-, \\ H_{\alpha_3} &= \alpha_3 \psi_{1,L}^{\dagger} \psi_{1,R} \psi_{2,L}^{\dagger} \psi_{2,R} + h.c. \\ &\sim \alpha_3 \cos 2\sqrt{2\pi} \phi_+. \end{aligned} \quad (22)$$

In summary, the full form of Hamiltonian is given by

$$\begin{aligned} H &= \sum_{l=\pm} \frac{v_l}{2} [K_l (\partial_x \phi_l)^2 + \frac{1}{K_l} (\partial_x \theta_l)^2] + \alpha_1 \cos 2\sqrt{2\pi} \phi_- \\ &\quad + \alpha_2 \cos 2\sqrt{2\pi} \theta_- + \alpha_3 \cos 2\sqrt{2\pi} \phi_+ \end{aligned} \quad (23)$$

B. Conditions for BSPT phase

We first consider symmetry operations of our Hamiltonian in more details. The charge conservation $U(1)_c$,

pseudo-spin symmetry $U(1)_m$, time-reversal symmetry \mathcal{T} and out-of-plane mirror symmetry M_z can be defined as

$$\begin{aligned} U(1)_c(\alpha) \begin{pmatrix} \phi_l \\ \theta_l \end{pmatrix} &= \begin{pmatrix} \phi_l \\ \theta_l - \frac{\alpha}{\sqrt{\pi}} \end{pmatrix} \\ U(1)_m(\alpha) \begin{pmatrix} \phi_l \\ \theta_l \end{pmatrix} &= \begin{pmatrix} \phi_l - \frac{\alpha}{\sqrt{\pi}} \\ \theta_l \end{pmatrix} \\ \mathcal{T} \begin{pmatrix} \phi_l \\ \theta_l \end{pmatrix} &= \begin{pmatrix} -\phi_l + \frac{\sqrt{\pi}}{2} \\ \theta_l - \frac{\sqrt{\pi}}{2} \end{pmatrix} \\ M_z \begin{pmatrix} \phi_l \\ \theta_l \end{pmatrix} &= \begin{pmatrix} \phi_l - \frac{\sqrt{\pi}}{2} \\ \theta_l \end{pmatrix}, \end{aligned} \quad (24)$$

respectively, where $l = 1, 2$. From Eq. (24), it is easy to see that $\theta_+ = \frac{1}{\sqrt{2}}(\theta_1 + \theta_2)$ carries the $U(1)_c$ charge, and ϕ_+ carries the $U(1)_m$ charge. We find that H_{α_1} and H_{α_2} preserve all the four symmetries, while H_{α_3} breaks $U(1)_m$ symmetry and preserves the mirror symmetry M_z . In the Appendix, we will show that H_{α_3} can originate from the standard Coulomb exchange interaction. Therefore, we conclude that a general Coulomb interaction reduces the symmetry of the 2D TMKI system from $U(1)_c \times U(1)_m \times M_z \rtimes \mathcal{T}$ to $U(1)_c \times M_z \rtimes \mathcal{T}$.

The existence of H_{α_3} is the key difference between our model and the interacting bilayer graphene model in Ref. [35]. In the bilayer graphene system, the BSPT phase is protected by $U(1)_c \times U(1)_s$ symmetry. Spin conservation symmetry $U(1)_s$ is preserved because (1) the spin-orbit coupling (SOC) effect is negligible and (2) the Coulomb interaction conserves total spin. In our TMKI system, the pseudo-spin symmetry $U(1)_m$ is playing the same role as the $U(1)_s$ symmetry in the bilayer graphene system. However, strong SOC exists in our system and the Coulomb interaction does not respect the pseudo-spin symmetry $U(1)_m$ due to the H_{α_3} term (Refer to the appendix for more details). If H_{α_3} is irrelevant, $U(1)_m$ symmetry will be recovered under renormalization group (RG) flow. As a result, the $U(1)_c \times U(1)_m$ symmetry protected BSPT phase will emerge, in analogy to the case studied in Ref. [35]. If H_{α_3} is relevant, the $U(1)_c \times U(1)_m$ symmetry will be explicitly broken even at low energy. However, one might still wonder whether the remaining mirror symmetry M_z can play the same role as the $U(1)_m$ in protecting a BSPT phase. Next we will study the RG flow of the $H_{\alpha_{1,2,3}}$ terms.

In our TMKI system, the decoupled Hamiltonians for ϕ_- and ϕ_+ are

$$\begin{aligned} H_{\phi_-} &= \frac{v_-}{2} [K_- (\partial_x \phi_-)^2 + \frac{1}{K_-} (\partial_t \phi_-)^2] + \alpha_1 \cos(2\sqrt{2\pi} \phi_-), \\ H_{\phi_+} &= \frac{v_+}{2} [K_+ (\partial_x \phi_+)^2 + \frac{1}{K_+} (\partial_t \phi_+)^2] + \alpha_3 \cos(2\sqrt{2\pi} \phi_+). \end{aligned} \quad (25)$$

The scaling dimensions of α_1 and α_3 are

$$\begin{aligned}\Delta(\alpha_1) &= \frac{(2\sqrt{2\pi})^2}{4\pi K_-} = \frac{2}{K_-}, \\ \Delta(\alpha_3) &= \frac{(2\sqrt{2\pi})^2}{4\pi K_+} = \frac{2}{K_+}.\end{aligned}\quad (26)$$

From Eq. (21), we find that when $g_1 > g_2 > 0$, both K_- and K_+ are greater than 1. Therefore, both interaction terms ($H_{\phi_{\pm}}$) are relevant. In the strong coupling limit, ϕ_- and ϕ_+ are pinned to

$$\begin{aligned}\phi_+ &= \frac{(2n+1)\pi}{2\sqrt{2\pi}} \\ \phi_- &= \frac{(2m+1)\pi}{2\sqrt{2\pi}},\end{aligned}\quad (27)$$

with $n, m \in \mathbb{Z}$ to minimize the cosine terms. Correspondingly, we have

$$\begin{aligned}\phi_1 &= \frac{(n+m+1)\sqrt{\pi}}{2} \\ \phi_2 &= \frac{(n-m)\sqrt{\pi}}{2}.\end{aligned}\quad (28)$$

By choosing $n = m = 0$, we arrive at $\phi_1 = \frac{\sqrt{\pi}}{2}, \phi_2 = 0$. The mirror symmetry operation will change ϕ_1 and ϕ_2 to $\phi'_1 = 0, \phi'_2 = -\frac{\sqrt{\pi}}{2}$ with $n = -1, m = 0$. Therefore, (ϕ_1, ϕ_2) and (ϕ'_1, ϕ'_2) are two degenerate states that are connected by mirror symmetry. In this case, both fermionic and bosonic degrees of freedom are explicitly gapped on the boundary. We can define a set of order parameter:

$$\begin{aligned}\Delta_{I,1} &= \langle \psi_{1,R}^\dagger \psi_{1,L} \rangle \sim \langle e^{-2i\sqrt{\pi}\phi_1} \rangle \\ \Delta_{I,2} &= \langle \psi_{2,R}^\dagger \psi_{2,L} \rangle \sim \langle e^{-2i\sqrt{\pi}\phi_2} \rangle.\end{aligned}\quad (29)$$

When ϕ_+ and ϕ_- fields are pinned, $\Delta_{I,l=1,2}$ acquires a non-vanishing expectation value which corresponds to the spontaneous mirror symmetry breaking (MSB).

When $g_2 > g_1 > 0$, $K_- < 1$ and $K_+ > 1$, the terms $\alpha_3 \cos 2\sqrt{2\pi}\phi_+$ and $\alpha_2 \cos 2\sqrt{2\pi}\theta_-$ are relevant, which pins ϕ_+ and θ_- to the following values

$$\begin{aligned}\phi_+ &= \frac{(2n'+1)\pi}{2\sqrt{2\pi}} \\ \theta_- &= \frac{(2m'+1)\pi}{2\sqrt{2\pi}},\end{aligned}\quad (30)$$

with $n', m' \in \mathbb{Z}$. This also gaps out all the bosonic degrees of freedom at the boundary. In this case, we need to define a new set of order parameter as

$$\begin{aligned}\Delta_{II,1} &= \langle \psi_{1,R}^\dagger \psi_{2,L} \rangle \sim \langle e^{-i\sqrt{2\pi}(\phi_+ - \theta_-)} \rangle \\ \Delta_{II,2} &= \langle \psi_{2,R}^\dagger \psi_{1,L} \rangle \sim \langle e^{-i\sqrt{2\pi}(\phi_+ + \theta_-)} \rangle,\end{aligned}\quad (31)$$

to characterize this MSB phase.

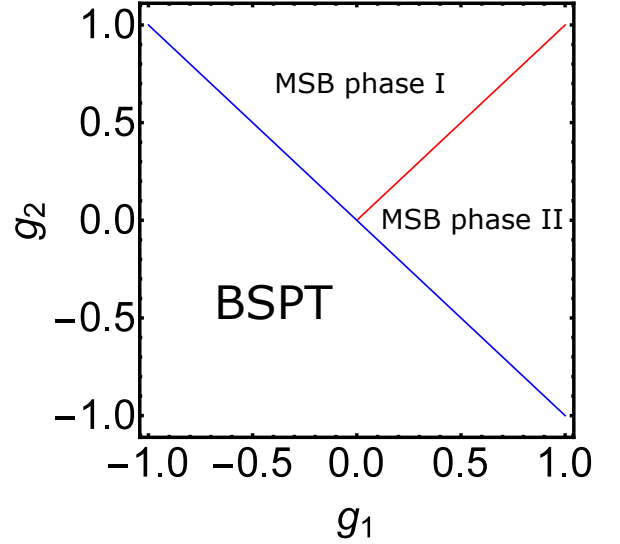


FIG. 4: Topological phase diagram of BSPT is plotted. Blue line ($K_+ = 1$) is the topological phase transition that separates the BSPT phase and trivial phases. Red line is a first order phase transition that separates two trivial MSB (mirror symmetry breaking) phases.

In general, due to the coexistence of $\alpha_1 \cos 2\sqrt{2\pi}\phi_-$ and $\alpha_2 \cos 2\sqrt{2\pi}\theta_-$, the anti-bonding bosonic degree of freedom is always gapped out for any value of K_- (except for the free case with $K_- = 1$). To guarantee the bonding bosonic mode is gapless, the system should satisfy the condition

$$g_1 + g_2 < 0, \quad (32)$$

which corresponds to attractive interaction. This condition implies that H_{α_3} is irrelevant. Under this condition, $U(1)_m$ symmetry is recovered in the infrared limit and can protect a BSPT phase together with the $U(1)_c$ symmetry, in analogy to the discussion in Ref. [35].

Based on the discussion above, we have mapped out the phase diagram of edge states in a TMKI, as shown in Fig. 4, where $K_+ = 1$ (blue line) separates the gapless edge states and MSB phases, and thus corresponds to a Kosterlitz-Thouless transition. In the entire MSB regime, all bosonic degrees of freedom are gapped out. In addition, this MSB regime can be further divided into two phases with different mirror-symmetry-breaking order parameters. The transition line ($K_- = 1$) that separates MSB phase I and MSB phase II is a first order phase transition.

C. Mirror parity domain wall in a mirror symmetry breaking phase

In the MSB regime, edge states are gapped out as a result of spontaneous MSB. As discussed in Ref. [53,54], domain wall structure of a gapped SPT phase possesses nontrivial degrees of freedom. In our model, the mirror

symmetry as a discrete Z_2 symmetry offers us an opportunity to construct a domain wall between phases which break the mirror symmetry differently. The mirror symmetry only affect ϕ_+ field (See Eq. (24)),

$$M_z \phi_+ = \phi_+ - \sqrt{\frac{\pi}{2}}. \quad (33)$$

According to the construction scheme in Ref. [53], the domain wall creation operator D_M is an exponential operator of θ_+ (the dual field of ϕ_+): $D_M = e^{iC\theta_+}$. The effect of the domain wall creation operator is

$$\begin{aligned} & D_M^{-1}(x)\phi_+(y)D_M(x) \\ &= e^{-iC\theta_+}\phi_+e^{iC\theta_+} \\ &= e^{-iC\theta_+}\phi_+[1 + \sum_{n=1}^{\infty} \frac{i^n C^n}{n!}(\theta_+)^n] \\ &= \phi_+(y) - C\Theta(x-y). \end{aligned} \quad (34)$$

Here we have used the commutation relation $[\phi_+(x), \theta_+(x')] = i\Theta(x' - x)$ with $\Theta(x - y)$ being the Heaviside step function. Since the domain wall operator connects two degenerate MSB vacua, we immediately obtain $C = \sqrt{\frac{\pi}{2}}$ while comparing with Eq. (33). The complete form of D_M is given by

$$D_M = e^{i\sqrt{\frac{\pi}{2}}\theta_+}. \quad (35)$$

Now we are ready to explore the properties of the above domain wall operator. The density operator j_0 is given by

$$j_0 = \frac{1}{\sqrt{\pi}}\partial_x(\phi_1 + \phi_2) = \sqrt{\frac{2}{\pi}}\partial_x\phi_+. \quad (36)$$

We consider a domain wall at x_0 and integrate j_0 across x_0 to obtain its charge accumulation of D_M as

$$Q(D_M) = \int_{x_0^-}^{x_0^+} j_0 dx = \int_{x_0^-}^{x_0^+} \sqrt{\frac{2}{\pi}}\partial_x\phi_+ dx = 1. \quad (37)$$

Therefore, D_M carries one unit charge. This can also be verified by performing the charge $U(1)$ transformation to D_M . On the other hand, we could test its response to TR symmetry operation \mathcal{T} :

$$\mathcal{T}^2 D_M = \mathcal{T} e^{i\sqrt{\frac{\pi}{2}}\theta_+ + i\frac{\pi}{2}} = -D_M. \quad (38)$$

Therefore, D_M transforms exactly like a spinful fermion under \mathcal{T} . Thus, we conclude that a domain wall D_M carries a charge-1 spinful fermion.

D. K matrix formulation of BSPT in interacting TMKIs

K matrix formulation has successfully been applied to the classification of SPT phases⁵⁵. In this section, we

connect our discussion based on standard Luttinger liquid language to the well known K matrix formulation, and explicitly construct the K matrix for a bosonic SPT phase in our system. To start with, we introduce a different yet equivalent Abelian bosonization scheme (compared to Eq. (15)) as

$$\begin{aligned} \psi_{l,R} &\sim e^{i\chi_{l,R}} \\ \psi_{l,L} &\sim e^{-i\chi_{l,L}}, \end{aligned} \quad (39)$$

while the definition of dual variables are modified as

$$\begin{aligned} \phi_l &= \chi_{l,R} + \chi_{l,L} \\ \theta_l &= \chi_{l,R} - \chi_{l,L}, \end{aligned} \quad (40)$$

with an extra sign factor in the definition of θ_l field for future convenience. In the Lagrangian form, our Hamiltonian is transformed to:

$$\mathcal{L} = \frac{1}{4\pi}(K_{IJ}\partial_t\chi_I\partial_x\chi_J - V_{IJ}\partial_x\chi_I\partial_x\chi_J), \quad (41)$$

where $\chi = (\chi_{1,R}, \chi_{1,L}, \chi_{2,R}, \chi_{2,L})^T$. Matrix V is determined by the Hamiltonian of the system, the form of which is not interesting to us. The K matrix of the system is given by

$$K = \begin{pmatrix} 1 & 0 & 0 & 0 \\ 0 & -1 & 0 & 0 \\ 0 & 0 & 1 & 0 \\ 0 & 0 & 0 & -1 \end{pmatrix}, \quad (42)$$

where a positive (negative) eigenvalue of K corresponds to a right (left) mover state. In the earlier discussions, we first re-express χ fields in terms of bosonic dual fields ϕ_l and θ_l ($l=1,2$) and then make a linear combination of these new dual fields to define the bonding and antibonding fields ϕ_{\pm} and θ_{\pm} . Here we describe the above process in a more compact way by introducing a set of vectors l_i ($i = 1, 2, 3, 4$):

$$\begin{aligned} \Psi_1 &= \phi_+ = l_1^T \chi = \frac{1}{2}(1, 1, 1, 1)\chi \\ \Psi_2 &= \theta_+ = l_2^T \chi = \frac{1}{2}(1, -1, 1, -1)\chi \\ \Psi_3 &= \phi_- = l_3^T \chi = \frac{1}{2}(1, 1, -1, -1)\chi \\ \Psi_4 &= \theta_- = l_4^T \chi = \frac{1}{2}(1, -1, -1, 1)\chi. \end{aligned} \quad (43)$$

With these vectors, we can rewrite our Lagrangian under this new bases $\Psi = (\Psi_1, \Psi_2, \Psi_3, \Psi_4)^T$. Define a transformation matrix $U = (l_1^T, l_2^T, l_3^T, l_4^T)$ and we have $\Psi = U\chi$. The new K matrix is

$$\tilde{K} = U^T K U = \begin{pmatrix} 0 & 1 & 0 & 0 \\ 1 & 0 & 0 & 0 \\ 0 & 0 & 0 & 1 \\ 0 & 0 & 1 & 0 \end{pmatrix}. \quad (44)$$

The block-diagonal form of \tilde{K} indicates that the two pairs of bosonic fields are completely decoupled. On one hand,

interaction will always gap out the bosonic anti-binding fields, which corresponds to the lower half block of \tilde{K} . On the other hand, when Luttinger parameter $K_+ < 1$ is satisfied, H_{α_3} is suppressed and $U(1)_m$ symmetry emerges. In this case, the bosonic bonding fields survive, and K effectively reduces to a 2×2 matrix:

$$K_{eff} = \begin{pmatrix} 0 & 1 \\ 1 & 0 \end{pmatrix}, \quad (45)$$

which is consistent with the K matrix for a bosonic SPT phase⁵⁵.

IV. CONCLUSION

In this paper, we have studied interacting topological phases in thin films of a TMKI, focusing on the bilayer system with the mirror Chern number ± 2 . At the single-particle level, we find that topological mirror insulator phases with different mirror Chern numbers (from ± 1 to

± 6) can be achieved by tuning film thickness and the hybridization between different layers. By introducing interaction into this system, bosonic SPT phases can be realized under certain parameter regime in TMKI films. Interaction can also drive the system into a MSB phase, in which a domain wall between different MSB order parameters can carry both charge and spin. Current experimental studies of TMKIs are focusing on bulk materials, such as bulk SmB_6 ^{39–41,56,57}, and we hope that our studies on interacting topological phases can motivate more experimental explorations on TMKI thin films⁵⁸.

V. ACKNOWLEDGEMENT

Rui-Xing Zhang would like to thank Jia-Bin Yu and Jian-Xiao Zhang for helpful discussions. C.-X.L. acknowledges the support from Office of Naval Research (Grant No. N00014-15-1-2675).

-
- ¹ X.-G. Wen, *Advances in Physics* **44**, 405 (1995).
² X. Chen, Z.-C. Gu, Z.-X. Liu, and X.-G. Wen, *Science* **338**, 1604 (2012).
³ X. Chen, Z.-C. Gu, Z.-X. Liu, and X.-G. Wen, *Physical Review B* **87**, 155114 (2013).
⁴ L. Fu, C. L. Kane, and E. J. Mele, *Physical Review Letters* **98**, 106803 (2007).
⁵ H. Zhang, C.-X. Liu, X.-L. Qi, X. Dai, Z. Fang, and S.-C. Zhang, *Nature physics* **5**, 438 (2009).
⁶ M. Z. Hasan and C. L. Kane, *Reviews of Modern Physics* **82**, 3045 (2010).
⁷ X.-L. Qi and S.-C. Zhang, *Reviews of Modern Physics* **83**, 1057 (2011).
⁸ L. Fu, *Physical Review Letters* **106**, 106802 (2011).
⁹ T. H. Hsieh, H. Lin, J. Liu, W. Duan, A. Bansil, and L. Fu, *Nature communications* **3**, 982 (2012).
¹⁰ K. Shiozaki and M. Sato, *Physical Review B* **90**, 165114 (2014).
¹¹ B. A. Bernevig, T. L. Hughes, and S.-C. Zhang, *Science* **314**, 1757 (2006).
¹² M. König, S. Wiedmann, C. Brüne, A. Roth, H. Buhmann, L. W. Molenkamp, X.-L. Qi, and S.-C. Zhang, *Science* **318**, 766 (2007).
¹³ C. Liu, T. L. Hughes, X.-L. Qi, K. Wang, and S.-C. Zhang, *Physical review letters* **100**, 236601 (2008).
¹⁴ I. Knez, R.-R. Du, and G. Sullivan, *Physical review letters* **107**, 136603 (2011).
¹⁵ Y. Chen, J. Analytis, J.-H. Chu, Z. Liu, S.-K. Mo, X.-L. Qi, H. Zhang, D. Lu, X. Dai, Z. Fang, et al., *Science* **325**, 178 (2009).
¹⁶ Y. Xia, D. Qian, D. Hsieh, L. Wray, A. Pal, H. Lin, A. Bansil, D. Grauer, Y. Hor, R. Cava, et al., *Nature Physics* **5**, 398 (2009).
¹⁷ D. Hsieh, Y. Xia, D. Qian, L. Wray, J. Dil, F. Meier, J. Osterwalder, L. Patthey, J. Checkelsky, N. Ong, et al., *Nature* **460**, 1101 (2009).
¹⁸ M. C. Rechtsman, J. M. Zeuner, Y. Plotnik, Y. Lumer, D. Podolsky, F. Dreisow, S. Nolte, M. Segev, and A. Szameit, *Nature* **496**, 196 (2013).
¹⁹ A. B. Khanikaev, S. H. Mousavi, W.-K. Tse, M. Kargarian, A. H. MacDonald, and G. Shvets, *Nature materials* **12**, 233 (2013).
²⁰ A. P. Schnyder, S. Ryu, A. Furusaki, and A. W. Ludwig, *Physical Review B* **78**, 195125 (2008).
²¹ L. Fidkowski and A. Kitaev, *Physical Review B* **81**, 134509 (2010).
²² L. Fidkowski and A. Kitaev, *Physical review b* **83**, 075103 (2011).
²³ X.-L. Qi, *New J. Phys.* **15**, 065002 (2013).
²⁴ H. Yao and S. Ryu, *Phys. Rev. B* **88**, 064507 (2013).
²⁵ S. Ryu and S.-C. Zhang, *Phys. Rev. B* **85**, 245132 (2012).
²⁶ Z.-C. Gu and M. Levin, arXiv:1304.4569 (2013).
²⁷ L. Fidkowski, X. Chen, and A. Vishwanath, *Phys. Rev. X* **3**, 041016 (2013).
²⁸ C. Wang and T. Senthil, *Phys. Rev. B* **89**, 195124 (2014).
²⁹ Y.-Z. You, Y. BenTov, and C. Xu, arXiv:1402.4151 (2014).
³⁰ Y.-Z. You and C. Xu, arXiv:1409.0168 (2014).
³¹ A. Vishwanath and T. Senthil, *Phys. Rev. X* **3**, 011016 (2013).
³² Y.-M. Lu and A. Vishwanath, *Phys. Rev. B* **86**, 125119 (2012).
³³ Z. Bi, A. Rasmussen, and C. Xu, *Phys. Rev. B* **91**, 134404 (2015).
³⁴ J. Wang, Z.-C. Gu, and X.-G. Wen, *Phys. Rev. Lett.* **114**, 031601 (2015).
³⁵ Z. Bi, R. Zhang, Y.-Z. You, A. Young, L. Balents, C.-X. Liu, and C. Xu, arXiv preprint arXiv:1602.03190 (2016).
³⁶ K. Slagle, Y.-Z. You, and C. Xu, *Phys. Rev. B* **91**, 115121 (2015), URL <http://link.aps.org/doi/10.1103/PhysRevB.91.115121>.
³⁷ Y.-Y. He, H.-Q. Wu, Y.-Z. You, C. Xu, Z. Y. Meng, and Z.-Y. Lu, *Phys. Rev. B* **93**, 115150 (2016), URL <http://link.aps.org/doi/10.1103/PhysRevB.93.115150>.
³⁸ M. Dzero, K. Sun, V. Galitski, and P. Coleman, *Physical*

- review letters **104**, 106408 (2010).
- ³⁹ M. Neupane, N. Alidoust, S. Xu, T. Kondo, Y. Ishida, D.-J. Kim, C. Liu, I. Belopolski, Y. Jo, T.-R. Chang, et al., Nature communications **4** (2013).
- ⁴⁰ J. Jiang, S. Li, T. Zhang, Z. Sun, F. Chen, Z. Ye, M. Xu, Q. Ge, S. Tan, X. Niu, et al., Nature communications **4** (2013).
- ⁴¹ N. Xu, X. Shi, P. Biswas, C. Matt, R. Dhaka, Y. Huang, N. Plumb, M. Radović, J. Dil, E. Pomjakushina, et al., Physical Review B **88**, 121102 (2013).
- ⁴² M. Xia, J. Jiang, Z. Ye, Y. Wang, Y. Zhang, S. Chen, X. Niu, D. Xu, F. Chen, X. Chen, et al., Scientific reports **4** (2014).
- ⁴³ N. Xu, C. Matt, E. Pomjakushina, G. Landolt, J.-Z. Ma, X. Shi, R. Dhaka, N. Plumb, M. Radovic, V. Strocov, et al., arXiv preprint arXiv:1405.0165 (2014).
- ⁴⁴ M. Neupane, S.-Y. Xu, N. Alidoust, G. Bian, D.-J. Kim, C. Liu, I. Belopolski, T.-R. Chang, H.-T. Jeng, T. Durakiewicz, et al., Physical review letters **114**, 016403 (2015).
- ⁴⁵ M. Ye, J. Allen, and K. Sun, arXiv preprint arXiv:1307.7191 (2013).
- ⁴⁶ M. Legner, A. Rüegg, and M. Sigrist, Physical review letters **115**, 156405 (2015).
- ⁴⁷ P. P. Baruselli and M. Vojta, Physical review letters **115**, 156404 (2015).
- ⁴⁸ M. Legner, A. Rüegg, and M. Sigrist, Physical Review B **89**, 085110 (2014).
- ⁴⁹ H. Isobe and L. Fu, Physical Review B **92**, 081304 (2015).
- ⁵⁰ T. Yoshida and A. Furusaki, Physical Review B **92**, 085114 (2015).
- ⁵¹ D. A. Abanin, P. A. Lee, and L. S. Levitov, Phys. Rev. Lett. **96**, 176803 (2006).
- ⁵² P. Maher, C. R. Dean, A. F. Young, T. Taniguchi, K. Watanabe, K. L. Shepard, J. Hone, and P. Kim, Nature Physics **9**, 154 (2013).
- ⁵³ X. Chen, Y.-M. Lu, and A. Vishwanath, Nature communications **5** (2014).
- ⁵⁴ Y.-M. Lu and D.-H. Lee, Physical Review B **89**, 205117 (2014).
- ⁵⁵ Y.-M. Lu and A. Vishwanath, Physical Review B **86**, 125119 (2012).
- ⁵⁶ D. Kim, J. Xia, and Z. Fisk, Nature materials **13**, 466 (2014).
- ⁵⁷ X. Zhang, N. Butch, P. Syers, S. Ziemak, R. L. Greene, and J. Paglione, Physical Review X **3**, 011011 (2013).
- ⁵⁸ J. Yong, Y. Jiang, D. Usanmaz, S. Curtarolo, X. Zhang, L. Li, X. Pan, J. Shin, I. Takeuchi, and R. L. Greene, Applied Physics Letters **105**, 222403 (2014).

Appendix A: Origin of H_{α_3}

In this section, we will show that H_{α_3} can originate from the standard Coulomb exchange interaction. This

result not only validates the physical meaning of H_{α_3} , but also implies that the Coulomb interaction generally breaks “pseudo-spin” $U(1)_m$ symmetry, despite the fact that it preserves both spin $U(1)_s$ symmetry and mirror symmetry M_z .

To start with, let us first express a right-moving edge state fermion operator $\psi_{l,R}$ in terms of bulk fermion operators $c_{\alpha,\sigma}$,

$$\psi_{l,R} = \sum_{\alpha} f_{l,\alpha} c_{\alpha,\uparrow} + \sum_{\beta} g_{l,\beta} c_{\beta,\downarrow}, \quad (\text{A1})$$

where $l = 1, 2$ and $c_{\alpha,\uparrow}$ and $c_{\beta,\downarrow}$ labels annihilation operators for the bulk states while $f_{l,\alpha}$ and $g_{l,\beta}$ are for the envelope wave functions of edge modes. Here α and β include both the orbital and layer indices for short. Let’s label the states $|\alpha(\beta), \sigma\rangle = c_{\alpha(\beta),\sigma}^{\dagger}|0\rangle$, where $|0\rangle$ is the vacuum state and $\sigma = \uparrow, \downarrow$. Since $\psi_{l,R}$ has a definite M_z mirror parity $+i$ while $f_{l,\alpha}$ and $g_{l,\beta}$ have no spatial dependence along the z -direction, we require both the states $|\alpha, \uparrow\rangle$ and $|\beta, \downarrow\rangle$ possessing mirror parity $+i$. On the other hand, since

$$M_z \begin{pmatrix} |\uparrow\rangle \\ |\downarrow\rangle \end{pmatrix} = \begin{pmatrix} +i & 0 \\ 0 & -i \end{pmatrix} \begin{pmatrix} |\uparrow\rangle \\ |\downarrow\rangle \end{pmatrix} \quad (\text{A2})$$

for spin parts, this indicates that $M_z|\alpha\rangle = +|\alpha\rangle$ and $M_z|\beta\rangle = -|\beta\rangle$.

TR symmetry transforms a right-mover $\psi_{l,R}$ to a left-mover $\psi_{l,L}$, giving rise to

$$\psi_{l,L} = \sum_{\alpha,\beta} f_{l,\alpha}^* c_{\alpha,\downarrow} - g_{l,\beta}^* c_{\beta,\uparrow}. \quad (\text{A3})$$

It is easy to see that both $c_{\alpha,\downarrow}$ and $c_{\beta,\uparrow}$ have mirror parity $-i$, which is consistent with that of $\psi_{l,L}$.

Now we are ready to rewrite the boundary interaction H_{α_3} , as well as $H_{\alpha_{2,3}}$, in terms of the bulk fermionic operators $c_{\alpha/\beta,\sigma}$. For simplicity, we only consider one α state and one β state in the decomposition of the edge state $\psi_{l,R/L}$. Let us first rewrite H_{α_3} with the help of Eq. (A1) and Eq. (A3) as

$$\begin{aligned}
H_{\alpha_3} &= \alpha_3 \sum_{k,k',q} \psi_{1,L,k+q}^\dagger \psi_{1,R,k} \psi_{2,L,k'-q}^\dagger \psi_{2,R,k'} + h.c. \\
&= \alpha_3 \sum_{k,k',q} (f_{1,\alpha} c_{\alpha,\downarrow,k+q}^\dagger - g_{1,\beta} c_{\beta,\uparrow,k+q}^\dagger) (f_{1,\alpha} c_{\alpha,\uparrow,k} + g_{1,\beta} c_{\beta,\downarrow,k}) \\
&\quad \times (f_{2,\alpha} c_{\alpha,\downarrow,k'-q}^\dagger - g_{2,\beta} c_{\beta,\uparrow,k'-q}^\dagger) (f_{2,\alpha} c_{\alpha,\uparrow,k'} + g_{2,\beta} c_{\beta,\downarrow,k'}) + h.c. \\
&= \alpha_3 \sum_{k,k',q} f_{1,\alpha} f_{2,\alpha} g_{1,\beta} g_{2,\beta} (c_{\alpha,\downarrow,k+q}^\dagger c_{\alpha,\uparrow,k'} c_{\beta,\uparrow,k'-q}^\dagger c_{\beta,\downarrow,k} + c_{\alpha,\downarrow,k'-q}^\dagger c_{\alpha,\uparrow,k} c_{\beta,\uparrow,k+q}^\dagger c_{\beta,\downarrow,k'}) \\
&\quad - f_{1,\alpha}^2 g_{2,\beta}^2 c_{\alpha,\downarrow,k+q}^\dagger c_{\alpha,\uparrow,k} c_{\beta,\uparrow,k'-q}^\dagger c_{\beta,\downarrow,k'} - g_{1,\beta}^2 f_{2,\alpha}^2 c_{\alpha,\downarrow,k'-q}^\dagger c_{\alpha,\uparrow,k'} c_{\beta,\uparrow,k+q}^\dagger c_{\beta,\downarrow,k} + h.c. \\
&= \alpha_3 \sum_{k,k',q} [2f_{1,\alpha} f_{2,\alpha} g_{1,\beta} g_{2,\beta} - (f_{1,\alpha}^2 g_{2,\beta}^2 + g_{1,\beta}^2 f_{2,\alpha}^2)] c_{\alpha,\downarrow,k+q}^\dagger c_{\alpha,\uparrow,k} c_{\beta,\uparrow,k'-q}^\dagger c_{\beta,\downarrow,k'} + h.c. \tag{A4}
\end{aligned}$$

By defining the spin operator as

$$\hat{S}_\alpha^i(q) = \sum_k \sum_{\sigma,\sigma'} c_{\alpha,\sigma,k+q}^\dagger S_{\sigma,\sigma'}^i c_{\alpha,\sigma',k}, \tag{A5}$$

with $i \in \{x, y, z\}$ and S^i is the corresponding Pauli matrix, H_{α_3} can be written in a compact form as

$$H_{\alpha_3} = J \sum_q \hat{S}_\alpha^+(q) \hat{S}_\beta^-(q) + h.c. \tag{A6}$$

where

$$S^\pm = S^x \pm iS^y$$

and

$$J = \alpha_3 [2f_{1,\alpha} f_{2,\alpha} g_{1,\beta} g_{2,\beta} - (f_{1,\alpha}^2 g_{2,\beta}^2 + g_{1,\beta}^2 f_{2,\alpha}^2)]. \tag{A7}$$

Eq. (A6) is exactly the Coulomb exchange interaction for the multi-orbital case. We would like to emphasize that this exchange process occurs between two electrons with opposite M_z mirror parities for the α and β parts in their wave functions. According to Eq. (A4), this type of Coulomb interaction breaks $U(1)_m$ symmetry, while preserving both $U(1)_s$ and M_z symmetry.